Integrated photonics for NASA applications

Michael Krainak*[a], Mark Stephen[a], Elisavet Troupaki[a], Sarah Tedder[b], Baraquiel Reyna[c], Jonathan Klamkin[d], Hongwei Zhao[d], Bowen Song[d], Joseph Fridlander[d], Minh Tran[d], John E. Bowers[d], Keren Bergman[e], Michal Lipson[e], Anthony Rizzo[e], Ipshita Datta[e], Nathan Abrams[e], Shayan Mookherjea[f], Seng-Tiong Ho[g], Qiang Bei[g], Yingyan Huang[h], Yongming Tu[h], Behzad Moslehi[i], James Harris[j], Andrey Matsko[k], Anatoliy Savchenkov[k], Guangyao Liu[l], Roberto Proietti[l], S. J. B. Yoo[l], Leif Johansson[m], Christophe Dorrer[n], Francisco R. Arteaga-Sierra[n], Jie Qiao[o], Songbin Gong[p], Tingyi Gu[q], Osgar John Ohanian III[r], , Xingjie Ni[s], Yimin Ding[s], Yao Duan[s], Hamed Dalir[t], Ray T. Chen[u], Volker J. Sorger[v], Tin Komljenovic[w]

[a]NASA-Goddard Space Flight Center, [b]NASA-Glenn Research Center,
[c]NASA Johnson Space Center, [d]Univeristy of California Santa Barbara ,[e]Columbia University,
[f]University of California San Diego, [g]Northwestern University, [h]OptoNet, [i]IFOS Inc.,
[j]Stanford University, [k]OEWaves Inc., [l]University of California-Davis, [m]Freedom Photonics Inc.,
[n]Aktiwave LLC,[o]Rochester Institute of Technology, [p]University of Illinois,
[q]University of Delaware, [r]Luna Innovations Incorporated, [s]Pennsylvania State University,
[t]Omega Optics, Inc.,[u]University of Texas at Austin,
[v]George Washington University, [w]Nexus Photonics

ABSTRACT

NASA is working with US industry and academia to develop Photonic Integrated Circuits (PICs) for: (1) Sensors (2) Analog RF applications (3) Computing and free space communications. The PICs provide reduced size, weight, and power that is critical for space-based systems. We describe recent breakthrough 3D monolithic integration of photonic structures, particularly high-speed graphene-silicon devices on CMOS electronics to create CMOS-compatible high-bandwidth transceivers for ultra-low power Terabit-scale optical communications. An integrated graphene electro-optic modulator has been demonstrated with a bandwidth of 30 GHz. Graphene microring modulators are especially attractive for dense wavelength division multiplexed (DWDM) systems. For space-based optical communication and ranging we have demonstrated generating a variable number of channels from a single laser using breadboard components, using a single-sideband carrier-suppressed (SSBCS) modulator driven by an externally-supplied RF tone (arbitrary RF frequency), a tunable optical bandpass filter, and an optical amplifier which are placed in a loop. We developed a Return--to-Zero (RZ) Differential Phase Shift Keying (DPSK) laser transmitter PIC using an InP technology platform that includes a tunable laser, a Semiconductor Optical Amplifier (SOA), high-speed Mach-Zehnder Modulator (MZM), and an electroabsorption (EAM) modulator. A Silicon Nitride (SiN) platform integrated photonic circuit suitable for a spectrally pure chip-scale tunable opto-electronic RF oscillator (OEO) that can operate as a flywheel in high precision optical clock modules, as well as radio astronomy, spectroscopy, and local oscillator in radar and communications systems is needed. We have demonstrated a low noise optical frequency combs generation from a small OEO prototypes containing very low loss (~1 dB) waveguide couplers of various shapes and sizes integrated with an ultrahigh-Q MgF2 resonators. An innovative miniaturized lab-on-a-chip device is being developed to directly monitor astronaut health during missions using ~3 drops of body fluid sample like blood, urine, and potentially other body fluids like saliva, sweat or tears. The first-generation system comprises a miniaturized biosensor based on PICs (including Vertical Cavity Surface Emitting Laser – VCSEL, photodetector and optical filters and biochemical assay that generates a fluorescent optical signal change in response to the target analyte.

Keywords: Times Roman, image area, acronyms, references
*michael.a.krainak@nasa.gov

Components and Packaging for Laser Systems V, edited by Alexei L. Glebov,
Paul O. Leisher, Proc. of SPIE Vol. 10899, 108990F · © 2019 SPIE
CCC code: 0277-786X/19/$18 · doi: 10.1117/12.2509808

1. INTRODUCTION

The development of photonic integrated circuits permits size, weight, power and cost reductions for spacecraft microprocessors, communication buses, processor buses, advanced data processing, free space communications and integrated optic science instrument optical systems, subsystems and components. This is particularly critical for small spacecraft platforms. NASA applications include:

(1) Integrated photonic sensors (physical, chemical and/or biological) circuits: NASA applications examples include (but are not limited to): Lab-on-a-chip systems for landers, Astronaut health monitoring, Front-end and back-end for remote sensing instruments including trace gas lidars Large telescope spectrometers for exoplanets using photonic lanterns and narrow band filters. On chip generation and detection of light of appropriate wavelength may not be practical, requiring compact hybrid packaging for providing broadband optical input-output and also, as means to provide coupling of light between the sensor-chip waveguides and samples, unique optical components (e.g. Plasmonic waveguides, microfluidic channel) may be beneficial.

(2) Integrated Photonic Circuits for Analog RF applications: NASA applications include new methods due to Size, Weight and Power improvements, passive and active microwave signal processing, radio astronomy and TeraHertz spectroscopy. As an example, integrated photonic circuits having very low insertion loss (e.g. ~1dB) and high spur free dynamic range for analog and RF signal processing and transmission which incorporate, for example, monolithic high-Q waveguide micro-resonators or Fabry-Perot filters with multi-GHz RF pass bands. These components should be suitable for designing chip-scale tunable opto-electronic RF oscillator and high precision optical clock modules.

(3) Integrated photonic circuits for very high speed computing and free space communications: Advanced computing engines that approach TeraFLOP per second computing power for spacecraft in a fully integrated combined photonic and electronic package. Free space communications downlink modems at the > 1 Terabit per second level for Near-Earth (Low-Earth Orbit to ground) and > 100 Mbps for > 1 AU distances.

2. NEW WAVEGUIDES

2.1 Low-Loss Waveguides Integrated with 2-D Materials

Silicon (Si) and silicon nitride (SiN) are quickly becoming dominant material platforms for integrated photonics due to their compatibility with the mature and low-cost CMOS process. Modulation in these platforms typically relies on the plasma dispersion effect where free carriers are injected into or extracted from the waveguide, changing the effective index and thus inducing a phase shift. However, the presence of additional carriers introduces loss through free carrier absorption. Under a NASA Early Stage Innovation grant, Columbia University has demonstrated a composite photonic platform with embedded monolayers of two dimensional (2D) materials in CMOS-compatible waveguides which enable pure phase shifting with no additional loss modulation.

Monolayer tungsten disulphide (WS_2) and molybdenum disulphide (MoS_2) exhibit strong changes in their optical properties with doping, which can be dynamically tuned by applying a bias voltage across the structure[1]. Embedding a 2D semiconductor monolayer above a waveguide induces an interaction with the evanescent tail of the propagating optical mode, and the electrically tunable monolayer doping changes the effective index of the mode which leads to a phase shift. Our tested device is fabricated (Fig. 1) by depositing monolayer WS_2 above a SiN waveguide, doping the monolayer by applying a bias voltage across the two electrodes after dispersing 3-4 μL of ionic liquid (1-butyl-1-methyl pyrrolidinium tris(pentafluoroethyl)trifluorophosphate ([P14+] [FAP-])) to top clad the devices. In response to the applied voltage, ions accumulate on the monolayer, which capacitively dopes the WS_2 with an average carrier density[2] of 1.5×10^{13} cm^{-2}.

To further characterize the phase efficiency of the device, we replaced the ionic liquid with a stack of Hafnia (HfO_2) and transparent conductive oxide, indium tin oxide (ITO), to form the TMD-HfO_2-ITO capacitor on the SiN waveguide. The phase shifter was integrated in both arms of a Mach Zehnder interferometer (MZI) with a path length difference between arms of 100 μm. We measured the change in effective index to be $\Delta n_{eff} = 7 \times 10^{-4}$ for an 8 V swing, which corresponds to a $V_\pi L$ of 1.33 V · cm, with a maximum absorption modulation of 0.005 dB/cm. The demonstrated light-matter interaction between the doped monolayer 2D materials and optical waveguide modes at telecommunication wavelengths

shows a promising path towards modulation and switching with low optical loss and low electrical power consumption in a CMOS-compatible platform.

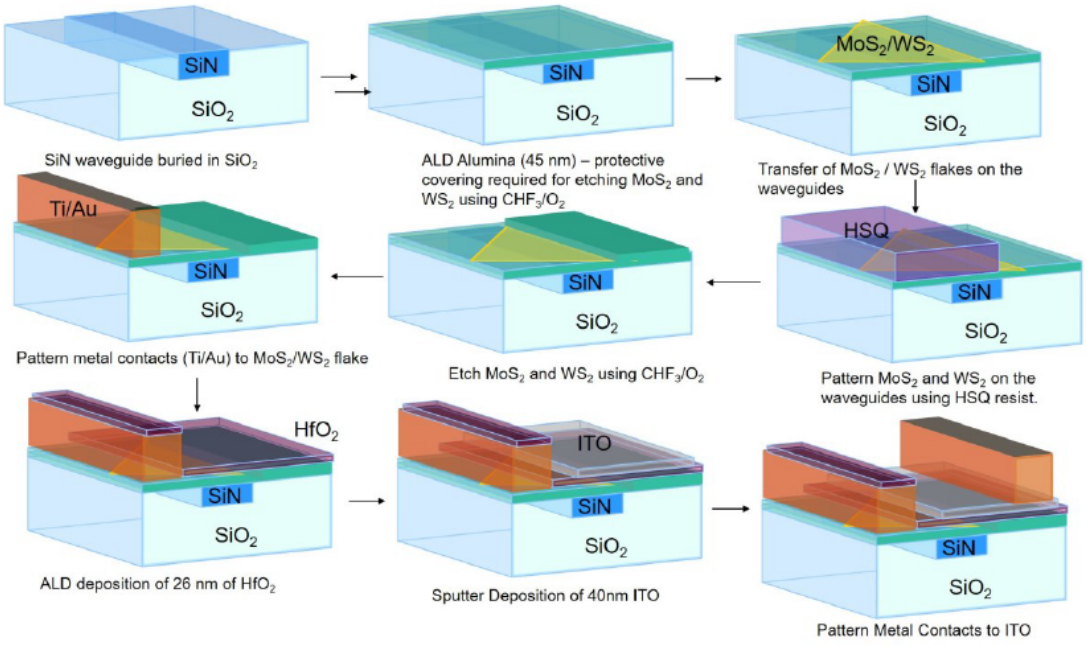

Fig. 1: Fabrication flow for integrated WS_2-HfO_2-ITO capacitor in the SiN platform.

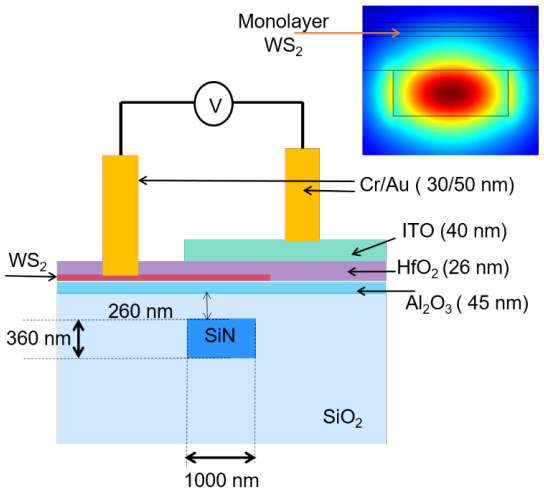

Fig. 2: Cross section of the fabricated device showing the composite monolayer WS_2-HfO_2-ITO capacitor on a SiN waveguide. The inset shows COMSOL simulation results, indicating a 0.03% interaction between the mode and the WS_2 monolayer.

2.2 Direct-Write using a femtosecond laser for waveguides in laser crystals

Aktiwave LLC and the Rochester Institute of Technology (RIT) are partners in an STTR to develop integrated theoretical models and experimental investigations in order to simulate and demonstrate femtosecond-laser-fabricated waveguides in crystalline dielectric materials. The numerical models will predict the refractive-index change resulting

from the propagation of intense femtosecond laser pulses inside the material. The influence of focal conditions and laser parameters (pulse energy, wavelength, repetition rate, focal spot size, and scanning speed) on waveguide quality and geometry will be theoretically and experimentally investigated via sensitivity studies. The index modulation will be evaluated for the three major waveguide-design configurations (Type I, II, and III) using matrices of laser parameters. The effectiveness of the three types of waveguide configurations will be compared for laser materials.

Numerical models have been established to describe femtosecond-laser beam propagation inside Nd:YAG and the resulting change in optical index that can be used to create waveguides. To model the peak fluence inside the Nd:YAG substrate at a desired depth via optimizing the input energy and focusing conditions, a numerical model based on the unidirectional-pulse-propagation-equation simulates the spot size and peak fluence evolution along the longitudinal direction, taking into account self-focusing by the Kerr effect and defocusing by plasma generation through multi-photon ionization (MPI). Increasing the numerical aperture, i.e. improving the focusing of the beam, results in higher peak fluence below the surface of the material (despite the energy drop because of MPI losses) compared to the case when only the input energy is increasing. But it is necessary to find a balance between these two parameters in order to control the required values of maximum peak fluence.

The femtosecond laser system at RIT has been upgraded to write waveguides with a high-average-power femtosecond fiber laser at 1030-nm and 515-nm. Waveguide writing has started on polished Nd:YAG crystals with a 0.5-NA microscope objective and pulse energy under 10 μJ, which are parameters identified via simulations. The geometric properties, mode profile, and linear losses of the written waveguides will be characterized to assess their suitability for an Nd:YAG laser.

3. INTEGRATED PHOTONICS FOR SPACE COMMUNICATION

Several NASA integrated photonics for space communication programs are described below.

3.1 RZ-DPSK Transmitter for Free Space Optical Communications

Photonic Integrated Circuits (PICs) offer reduced C-SWaP, eliminate interconnect losses, allow easy integration of built-in test capabilities, and are an attractive technology for space applications and miniature satellite platforms such as CubeSats.

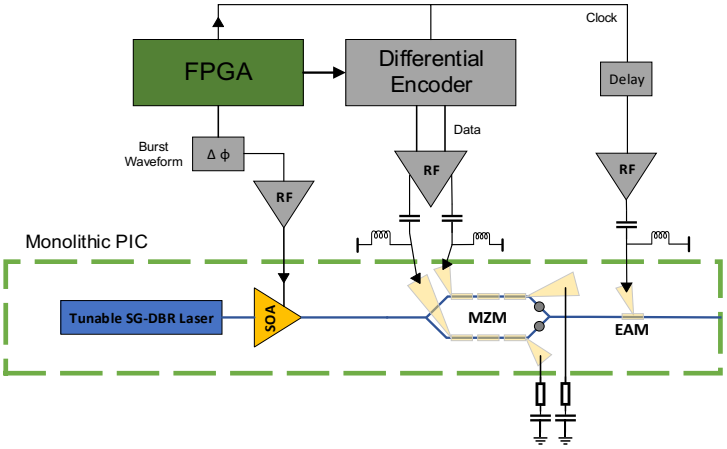

Figure 3. Transmitter Architecture

An RZ-DPSK Tx Architecture[3] allows straight-forward non-coherent detection with a delay line interferometer. The RZ clock encoding in optical envelope allows for minimized preamble and multi-rate transmission is possible with burst mode and an average power limited amplifier.

Under a NASA Early Stage Innovation and SBIR program, the University of California Santa Barbara and Freedom Photonics LLC have been developing the transmitter architecture shown in Figure 3. This PIC transmitter has an integrated tunable C-band sampled grating distributed Bragg reflector (SG-DBR) laser which is amplified by a semiconductor optical amplifier (SOA). The SOA is also used for generation of burst waveforms. The differentially driven Mach Zehnder Modulator (MZM) modulates the optical carrier with amplified differentially encoded binary

phase shift keying data. Tunable phase sections are available on each of the MZM's arms for optimal interferometer alignment. An electro-absorption modulator (EAM) pulse carver generates the RZ envelope. The EAM is driven by an amplified data clock, which requires delay control for optimal alignment with the data symbols.

Figure 4 shows the intensity profile of 1 Gbps and 2.5 Gbps DPSK (left and middle respectively) and RZ-DPSK modulated signal (right). To generate the DPSK signal, the MZM is biased at the null point. The EAM works as a pulse carver to generate a 50% duty cycle RZ-DPSK signal with an averaged 11 dB extinction ratio.

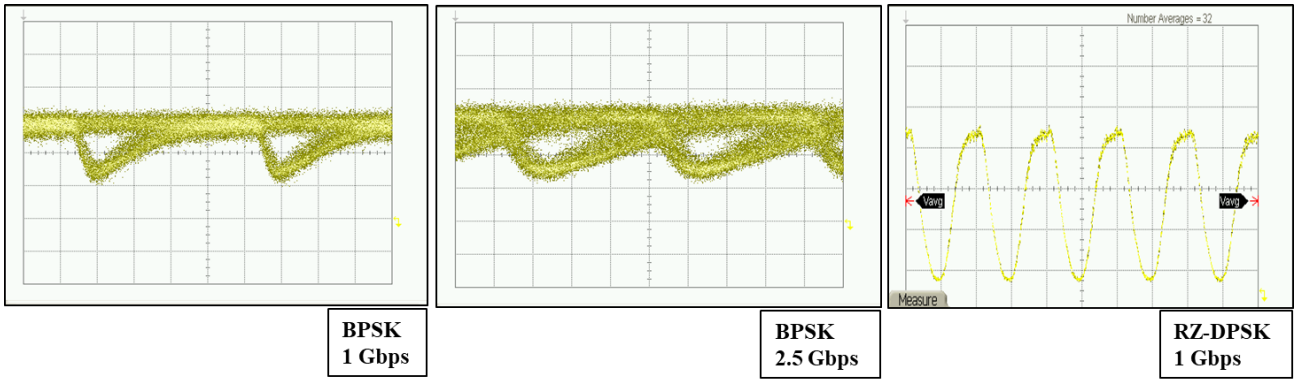

Figure 4. DPSK eye-diagrams at 1 Gbps with 200 ps/div (left), 2.5 Gbps with 100 ps/div (middle), and RZ-DPSK eye diagram at 1 Gbps with 500 ps/div (right).

3.2 Indium Phosphide Integrated Transmitter for Free Space Links

The indium phosphide (InP) photonic integrated circuits (PIC) transmitter consists of a widely tunable sampled grating distributed Bragg reflector (SGDBR) laser, a high-speed SOA, a MZM, and a high-power two-section SOA[4,5,6]. The active/passive integration technique utilizes an offset structure with a single p-cladding regrowth.

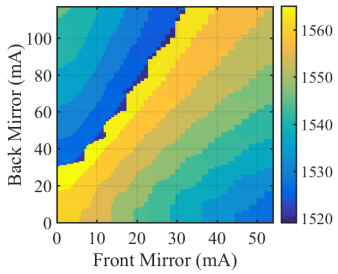

Figure 5. Emission wavelength (nm) as a function of currents applied to the front and back mirrors.

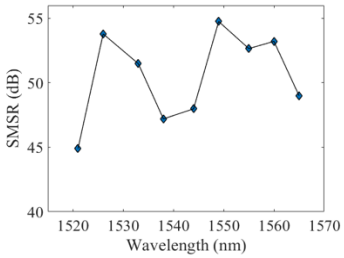

Figure 6. Measured side mode suppression ratio across the tuning range.

The emission wavelength of the transmitter can be tuned from 1521nm to 1565nm, covering more than the entire C-band. Figures 5 & 6 shows the tuning characteristics of the SGDBR laser with currents applied to the front and back mirror. Across the entire tuning range, the side mode suppression ratio is > 45 dB[5]. The eye diagrams for 1 Gbps and 3 Gbps non-return-to-zero (NRZ) on-off keying (OOK) modulation are demonstrated in Figure 7.

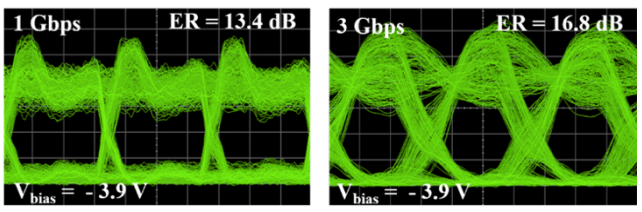

Figure 7. Eye diagrams for 1 Gbps and 3 Gbps NRZ OOK modulation.

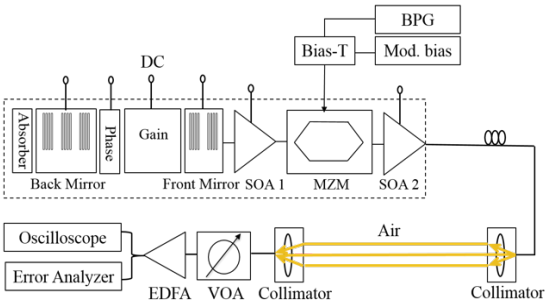

Figure 8. Schematic of free space optical link setup.

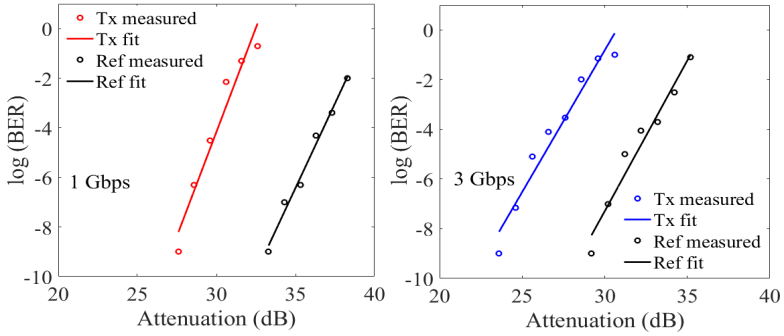

Figure 9. BER for 1 Gbps and 3 Gbps NRZ OOK transmission.

A free space optical link, as shown in Figure 8, was set up with the fabricated InP PIC transmitter[6]. With two identical commercial collimators, the optical signal was transmitted into air and then collected into to fiber. At the receiver side, an in-fiber variable optical attenuator was used to simulate the geometry attenuation of the free space optical link. Figure 9 shows bit error rate results as a function of the link attenuation at 1 Gbps and 3 Gbps, respectively. At 3 Gbps, link operates free of errors up to approximately 24 dB attenuation, corresponding to 180 m link length. With forward error correction, the equivalent link length is 300 m (28 dB attenuation).

3.3 Hybrid Integrated Silicon Laser

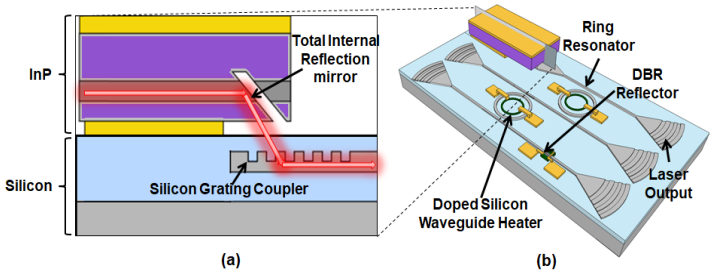

Fig. 10 (a) Side-view schematics of 3D integrated hybrid silicon laser; (b) Perspective view of tunable 3D SPECL with two intra-cavity ring resonators.

Although very promising as a PIC platform, integrated laser still remains as a bottleneck for silicon photonics. Under a NASA Early Career Faculty grant, a novel 3D hybrid integration technique for integrating lasers on silicon was proposed[7]. Figure 10(a) shows a side view schematic of the 3D hybrid integration approach where an indium phosphide (InP) reflective semiconductor optical amplifier (RSOA) with a high reflectivity (HR) coated back mirror and a TIR turning mirror is bonded to silicon. Light is coupled to the silicon waveguide through a vertical grating coupler. The RSOA can be bonded P-side down to the silicon substrate for efficient heat removal from the active region. This is particularly attractive for high power integrated lasers because it leads to lower thermal impedance, and in turn higher efficiency and potentially lower relative intensity noise (RIN). The integration is carried out in a backend step, which avoids co-fabrication of incompatible materials. The 3D hybrid integration approach also allows III-V PICs to be bonded to silicon interposers for large-scale electronic-photonic integration.

Figure 10(b) shows the perspective view of a SPECL with two tunable ring filters. The tunable DBR mirrors provide filtered feedback and additional phase control. The silicon chips used in this work were fabricated at the Interuniversity Microelectronics Centre. The InP RSOAs were fabricated using an etched-facet process and the gain section length was 500 µm. Thermocompression was utilized with a bond temperature of 350ºC and a force of approximately 20 N. Figure 11(a) shows a microscope image of the fabricated SPECL. LIV characteristics are measured at room temperature and the results are shown in Figure 11(b). RIN and laser linewidth measurements were also performed for the SPECL. RIN spectra at various pump currents are shown in Figure 11(c). A RIN peak of -132 dB/Hz was measured at a current of 70

mA. The inset shows the square of the relaxation resonance frequency as a function of current (less the threshold current), demonstrating an expected linear relationship. The self-heterodyne method was used to extract the laser linewidth of the SPECL. A Lorentzian fit was applied to precisely evaluate the laser linewidth. A 3-dB beat of 1.5 MHz was measured at a pump current of 104 mA as shown in Figure 11(d). A factor of three improvement is experimental demonstrated. This ability to bond an active laser or RSOA chip directly to the silicon substrate would enable higher laser efficiency and high-temperature operation. This is also attractive for free space applications that require high performance, and especially high-power integrated laser sources.

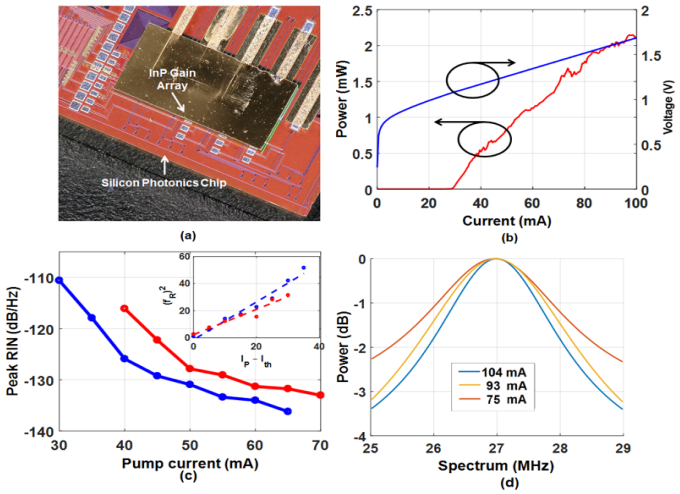

Figure 11. (a) Optical microscope image of 3D SPECL; (b) LIV characteristics of the SPECL; (c) Superimposed RIN spectra at various currents for SPECL with inset showing square of relaxation resonance frequency (fR2) versus IP – Ith; (d) Superimposed linewidth measurements spectra at various currents.

3.4 Ultra-Low Power CMOS-Compatible Integrated-Photonic Platform for Terabit-Scale Communications

Current state-of-the-art free space laser links used for satellite communications are severely limited in speeds primarily due to the high power consumption of the optical transceivers. We exploit recent breakthrough 3D monolithic integration of photonic structures, particularly high-speed graphene-silicon devices on CMOS electronics. In this way, under a NASA Early Stage Innovation grant, Columbia University is creating CMOS-compatible high-bandwidth transceivers for ultra-low power Terabit-scale optical communications. The new platform can enable implementation of graphene-silicon structures with unprecedented data modulation speeds, offering an optical space communications infrastructure within a compact power envelope.

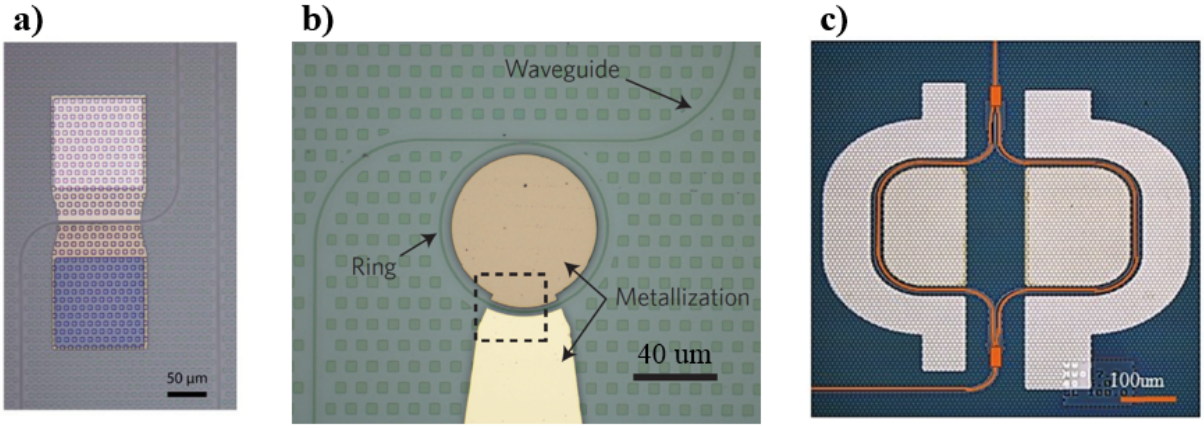

Figure 12. a) Linear graphene absorption modulator b) Integrated graphene microring modulator c) Graphene phase modulator with minimal absorption variation

The combination of high carrier mobility and broadband absorption makes graphene an ideal material to develop into integrated modulators[8]. By placing a graphene capacitor directly above a silicon nitride waveguide, the absorption in the waveguide can be modulated with an applied voltage to the capacitor (Figure 12a.). The absorption modulation from the integrated graphene modulator is inherently linear and was demonstrated to have a spurious free dynamic range[9] of 100 dBc/Hz$^{2/3}$. By placing the capacitor above a silicon nitride microring, the modulated voltage to the graphene capacitor varies the round-trip loss in the ring, which in turn varies the Q of the ring. As the Q of the ring is modulated, the transmission in the bus waveguide will also be modulated. Such an integrated graphene electro-optic modulator has been demonstrated[10] with a bandwidth of 30 GHz (Figure 12b). Integrated graphene modulators were also fabricated (Figure 12c) to operate in a phase modulation regime with minimal effects on the absorption, demonstrating the potential for graphene modulators to be employed for both amplitude and phase modulation[11].

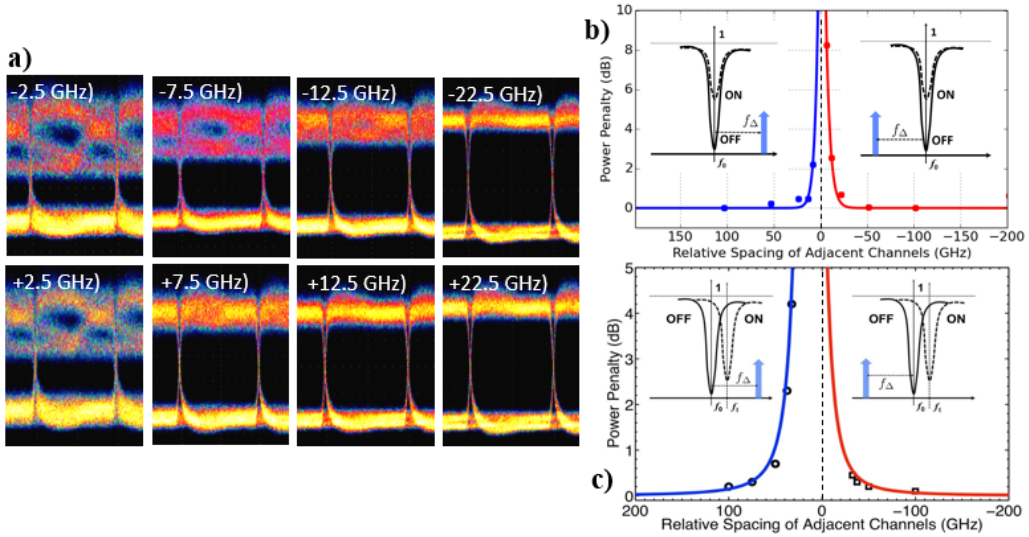

Figure 13. a) Eye diagrams with various channel spacings for the integrated graphene microring modulator, demonstrating the potential for DWDM b) The power penalty curve for various channel spacings of the graphene microring modulator, indicating minimal intermodulation crosstalk at channel spacings of 25 GHz c) The power penalty curve for a traditional silicon photonic modulator, indicating the necessity of 100 GHz channel spacings

In addition to the promise of high speed modulation, integrated graphene microring modulators are especially attractive for dense wavelength division multiplexed (DWDM) systems. While the applied voltage to the graphene capacitor varies the Q of the ring, it has a negligible effect on the index of refraction, producing no spectral shift. Traditional silicon photonic microring modulators achieve their modulation through modulating the concentration of free carriers, which changes the index of refraction and shifts the resonance spectrum. This resonance shift places a limit on the channel spacing in DWDM systems; channels placed too close together will degrade the modulation quality through intermodulation crosstalk. The lack of a resonance shift in graphene microring modulators means channels in a DWDM system can be placed closer together than silicon microring modulators for a comparable amount of intermodulation crosstalk. Experimental analysis of the intermodulation crosstalk for the graphene microring modulators show that 25 GHz channel spacings are supported (Figure 13), compared to 100 GHz channel spacings for a more traditional silicon photonic microring modulator[12].

3.5 Integrated Photonics for Adaptive Discrete Multi-Carrier Space-Based Optical Communication and Ranging

In many space-based optical communications applications of relevance to NASA science and engineering objectives, the presented data traffic is highly bursty, depending on highly variable physical parameters such as transmitter-receiver alignment, vehicle trajectories, atmospheric conditions etc. We will benefit from being able to enhance the data rate of optical communications to the Terabit-per-second regime when demanded, and scale back to a lower, more energy efficient communications rate at other times. Using modern silicon photonics, under a NASA Early Stage Innovation grant, the University of California San Diego (UCSD) is developing a microchip technology that can serve these objectives, and presents a roadmap for optical communications chipsets for communication and/or relay network in near-Earth space at wavelengths near 1550 nm that can scale up to 500 Gbit/s, or beyond.

UCSD is developing an electro-optic modulator that is capable of very-high bandwidth (>110 GHz already demonstrated) and is compatible with the silicon photonics manufacturing process flow. This modulator is based on hybrid silicon photonics, in which a thin film of lithium niobate is bonded on top of a (height-reduced) silicon waveguide, to form a hybrid mode. Bringing lithium niobate, a traditional EOM material for space applications, into the modern hybrid fabrication flow (at a US-based foundry, the Sandia National Labs) is a key innovation that is expected to benefit many applications. The input-output and other optical components (e.g., splitters, combiners) are realized in silicon photonics, and light makes an inter-layer transition to the LN layer for the ultra-high-speed modulator. Because of this wafer-scale integration with silicon, micro-chip-sets can be envisioned which support dozens of 100 GHz modulators with integrated waveguides, for truly scalable very high bit-rate communications with orders-of-magnitude reductions in size, weight, and energy consumption.

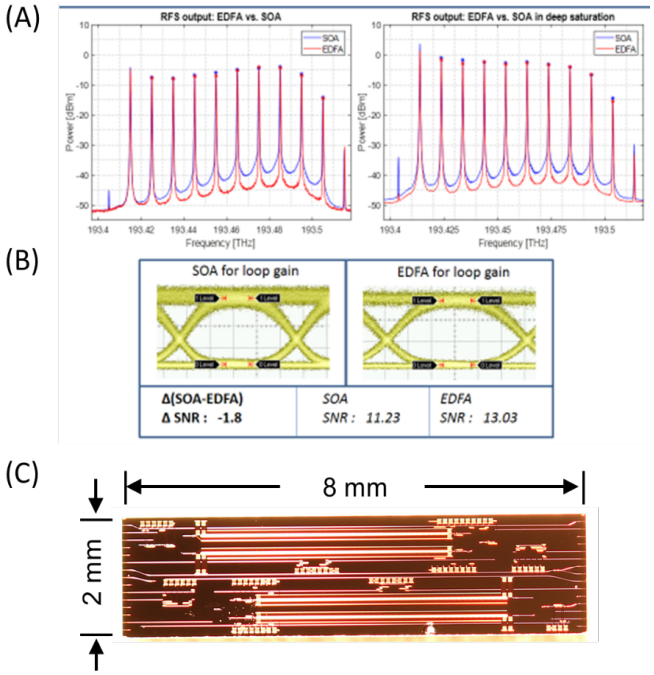

Figure 14. a) Breadboard demonstration of multi-tone generation (9 tones, 10 GHz spacing) using a recirculating loop architecture driven by a single seed laser. b) For a test case of 10 Gbit/s NRZ modulation per tone, a comparison was performed of eye diagrams and signal quality based on two different amplifier choices in the loop. c) Photograph of silicon photonic microchip, which integrates the single-sideband suppressed carrier modulator, tunable optical bandpass filters, couplers, polarization filters, monitoring and stabilization points, and other required components except the amplifier and the seed laser.

This project has demonstrated generating a variable number of channels from a single laser (Figure 14a) using breadboard components, using a single-sideband carrier-suppressed (SSBCS) modulator driven by an externally-supplied RF tone (arbitrary RF frequency), a tunable optical bandpass filter, and an optical amplifier which are placed in a loop[13]. A microchip version (Figure 14c) which uses silicon photonics technology for all the components (except the optical amplifier, which still relies on III-V semiconductors, for which care should be taken to avoid nonlinear wave mixing[14]) has been fabricated using a silicon foundry process (Sandia National Labs, Albuquerque, NM) and is currently being tested at UC San Diego.

Design innovation and the judicious use of modern semiconductor fabrication technologies are both important in overcoming the limitations of traditional integrated optics. Hybrid optical amplifiers and lasers (III-V lasers bonded to silicon waveguides) and hybrid electro-optic modulators (Lithium Niobate thin film modulators bonded to silicon waveguides) have also been shown by UC San Diego researchers and their collaborations, in both cases, using wafer-scale silicon photonics fabrication[15]. The advantage of a single-laser approach for generating a variable number of optical carriers is to avoid the potential un-reliability of multiple lasers on the same die, and achieve granular control over the number of carriers, which will enable user-defined dynamic communications rate adjustment over a very wide

range. The recirculating-loop approach may result in a useful programmable transceiver device architecture not only for NASA communications applications, but other optical systems as well.

3.6 Ranging Compact Robust Integrated PPM Laser Transceiver Chip Set with High Reconfigurability

The realization of integrated laser data transmitter chip with the ability to transmit reconfigurable multiple wavelength channels and realize pulse-position modulation (PPM) with a total data rate of 10-100Gbps is of interest for space applications. Under a NASA Early Stage Innovation grant, Northwestern University and Optonet Inc. designed and fabricated a wavelength division multiplexed transmitter chip and corresponding receiver chip by using an integrated compact diffraction grating with high wavelength resolution, called super compact grating (SCG), as the wavelength selection element. The SCG and passive waveguides were made using the thin silicon layer on a SOI substrate.

The employment of many gain waveguides (with gain sections $GS_1..GS_n$), each to receive beam at a different diffraction angle from SCG, would enable lasing at multiple wavelength channels $\lambda_1..\lambda_n$, but with a common output at OM. Beam output from OM is then coupled to an output optical fiber. The gain section is realized by heterogeneous integration of InP based gain material layer on the surface of a silicon waveguide by wafer bonding technique[16]. Figure 16 shows an actual transmitter chip realized. Figure 17 shows an example of the laser output power vs current. Using ten wavelength channels at 1Gb/sec modulation rate per channel, 10Gb/sec data rate can be reached.

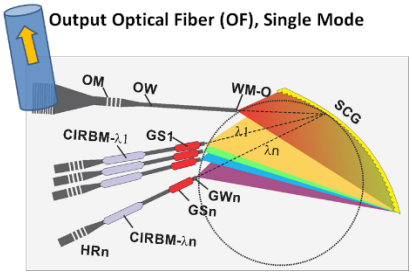

Figure 15. Transmitter chip geometry.

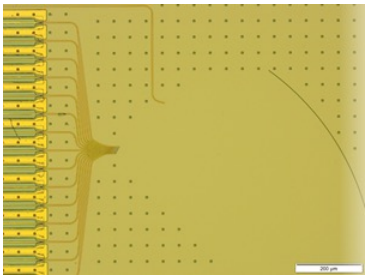

Figure 16. Transmitter chip realized.

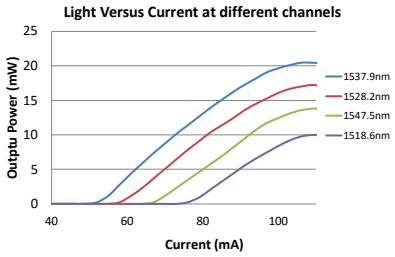

Figure 17. Lasing output.

Figure 15 shows the geometry of the transmitter chip cavity, formed by a linear Bragg grating (OM) that acts as the "output mirror", the SCG, and an optical gain waveguide (GW_n). GWn has a gain section (GSn) and a Bragg high reflector (HR_n) at the end of GW_n. A light beam from OM at a particular wavelength λ_n propagating toward SCG would be diffracted by SGC to GW_n. Reflector HRn would reflect the light back to SCG and then to OM, forming a closed cavity path. This cavity would give lasing at wavelength λ_n that is defined by the diffraction angle of the beam at SCG. PPM modulation of the laser beam is realized by directly modulating the gain section.

3.7 Hybrid Integration of Nonlinear Crystals on Silicon Photonics for Space Communication and Sensing

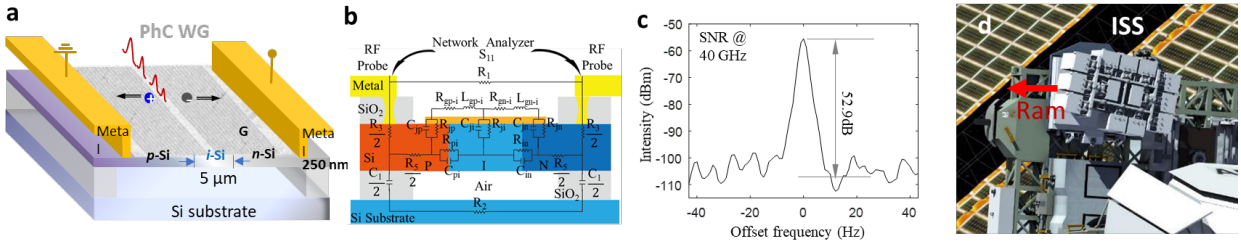

Figure 18. Back-end-of-line processing compatible G-Si ultrafast photodetector. a. A schematic diagram of the hybrid device configuration. b. small signal model analyzing the resistant-capacitance constant limitation of the direct contact hybrid device. c. Measured signal to noise ratio at 40 GHz modulation speed. d. Radiation test on International Space Station in 2019.

Under an Early Career Faculty grant, the University of Delaware is developing new scalable hybrid integration techniques that incorporate nonlinear crystal materials with standard CMOS silicon processing to realize low cost implantation of miniaturized optical instruments on chip. We will apply these new methods towards radiation hard nanoscale components towards high-speed on-chip optical communication subsystems. We design device configurations

that combine CMOS foundry fabricated advanced substrates and radiation hard materials with desired functionalities in direct contact with the atomically flat substrate, as well as engineer the interface quality for efficient optoelectronic conversions.

The hybrid graphene-silicon *p-i-n* junction photodiode device configuration has been developed and demonstrated for simultaneously addressing high speed (> 50 GHz) and low noise operation (Signal to noise ratio > 50 dB at 40 GHz modulation speed)[17]. Single layer graphene is transferred on to active Si photonics devices fabricated in CMOS foundry (Figure 18a-c). Atomically flat graphene surface on the silicon substrate ensures low optical propagation loss and efficient lateral transportation of photogenerated carriers on Graphene-silicon interface. The unique band alignment between graphene and doped silicon enables drift current dominant photocarrier collection in the two-dimensional junction. The electrical gain is obtained through both hot carrier effect on graphene-intrinsic silicon contact and carrier multiplication on graphene-doped silicon interface. As the optoelectronic device speed is constrained by both photocarrier transit time and resistance-capacitance time constant (RC constant) limit, we built a correspondent small signal model for the hybrid device[18,19]. Experimental results shew the RC constant limit of our device configuration can be 110 GHz. We have verified graphene's resistance towards low energy proton plasma exposure through the ground test, and preparing a six month robustness of the active silicon photonic devices on international space station on near earth orbit.

4. INTEGRATED PHOTONICS FOR SPACE SENSORS

Several NASA integrated photonics for space sensors programs are described below.

4.1 Optical Frequency Domain Reflectometry (OFDR) system-on-chip

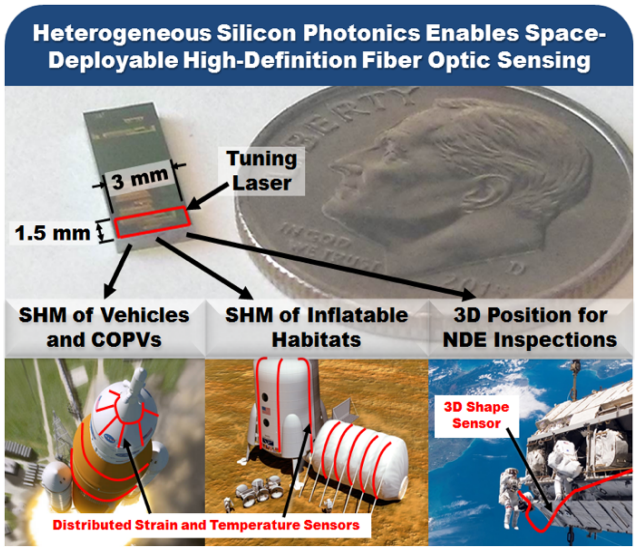

Figure 19. Luna's heterogeneous silicon photonic implementation of OFDR would impact many aerospace applications.

Through a NASA STTR (NNX17CG50P), Luna Innovations is developing an Optical Frequency Domain Reflectometry (OFDR) system-on-chip via heterogeneous silicon photonics. This will enable a minimal weight structural health monitoring (SHM) sensing system for space applications (Figure 19). What makes OFDR unique is the use of a swept laser and its ability to produce high spatial density measurements (< 1 mm between data points). Structural health monitoring of composite structures in space vehicles and space habitats would benefit from HD-FOS sensing, but the fiber optic interrogation system requires miniaturization for space launch.

As a first step towards this goal, a tunable laser prototype was fabricated by the University of California Santa Barbara (UCSB). Heterogeneous silicon photonics combines epitaxial layers of silicon, silicon nitride, and III-V semiconductor materials into a single photonic chip, which is manufactured using mature semiconductor processing techniques. The completed device occupies a small total area of 2.5 mm×0.5 mm (Figure 20, from [20]). It has a tuning range of 55 nm (1538 nm – 1593 nm). Near-60 dB SMSRs were achieved within 1557 nm – 1585 nm, while greater than 50 dB SMSRs

were seen across the whole tuning range. Figure 2(d) shows an example of ~52.5 kHz linewidth measured at 100 mA injection current and 1543 nm wavelength. A summary of the SMSR and spectral linewidth across the tuning range is shown in Figure 20(e). These linewidths are suitable for OFDR sensing and will be leveraged in the next phase of development.

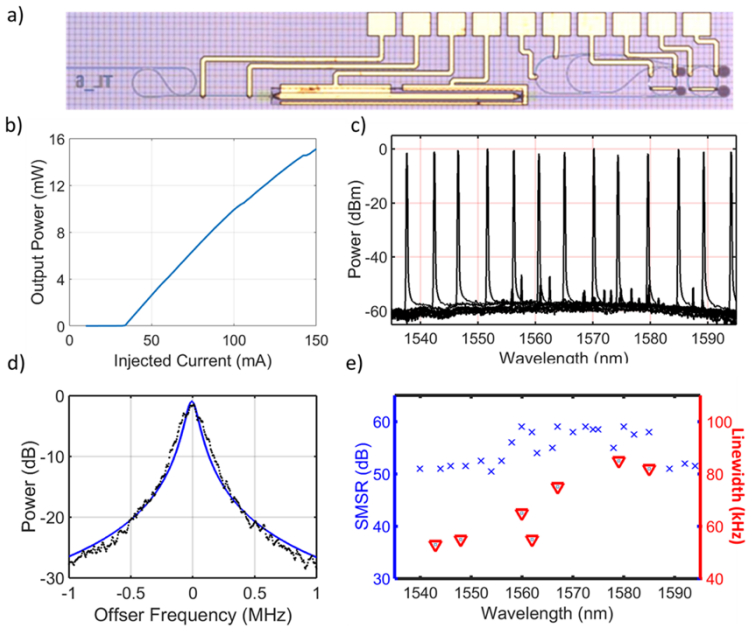

Figure 20. (a) Microscopic image of the fabricated tunable laser (b) LI curve measured with an on-chip detector, showing a threshold current of 34 mA (c) Wavelength tuning when the injection current to the gain section was 100 mA (d) Delayed self-heterodyne linewidth measurement (blue dots) and a Voigt fit (black line) shows a 3 dB Lorentzian linewidth of 52.5 kHz calculated from -20 dB points (e) Measured linewidths and side mode suppression ratios across the full tuning range.

4.2 Multifunctional Integrated Photonic Lab-on-a-Chip for Astronaut Health Monitoring

While widely used for terrestrial medical applications, handheld blood analyzers are not suitable for space missions due to the short shelf-life of their measurement cartridges as well their lack of clinical grade accuracy and sensitivity. Therefore, scientists researching the impact of spaceflight on humans often have access only to pre- and post-flight data. This also means that astronauts do not have a simple and reliable method to accurately and in real-time monitor key health parameters during spaceflight. Clearly, an *in situ* measurement capability would provide significant benefits both to operations and spaceflight factors research as well as in decision-making of managing astronauts' health.

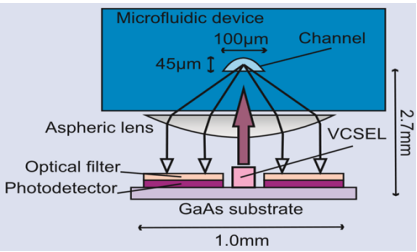

Figure 21. Integrated sensor schematic. [1]

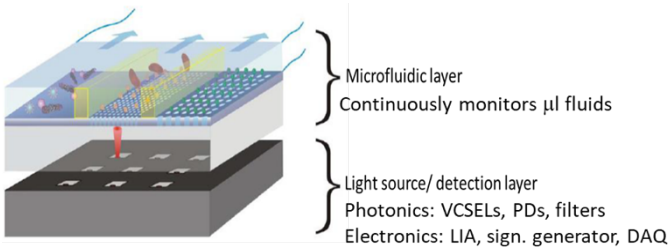

Figure 22. Multiplexed biochemical sensing platform.[3]

PIC-based biochemical sensors offer enhanced robustness and assay longevity compared with conventional portable analyzers. Under a NASA STTR program, IFOS Inc. and Stanford University are developing an innovative miniaturized *lab-on-a-chip* device is being developed to directly monitor astronaut health during missions using ~3 drops of body fluid sample like blood, urine[21], and potentially other body fluids like saliva, sweat or tears. The first-generation system comprises a miniaturized biosensor based on PICs (including Vertical Cavity Surface Emitting Laser – VCSEL,

photodetector and optical filters – as shown in Figure 1 and biochemical assay that generates a fluorescent optical signal change in response to the target analyte[22].

This approach will enable simultaneous, multiplexed measurement capability using integrated microfluidic circuitry or standard microfluidic samples slides from the medical industry – see Figure 2.

The initial focus is on measurement of total protein concentration in blood and urine, the level of which can be indicative of liver and kidney conditions, infections, and bone marrow disorders[21]. In experiments, a prototype lab-on-chip device demonstrated measurement performance better than gold-standard benchtop instruments including large benchtop spectrophotometer colorimetric assays[23]. In follow-on work, as was shown in the model in Figure 22, the sensor capabilities will be extended to for multiplex detection of other body fluids from which a number of analytes will be explored in accordance with NASA Human Research Program Exploration Medical Capability Element priorities. As an additional benefit, this PIC biosensor platform being an efficient and fieldable generic optical transducer, could be used cross-functionally to monitor water quality and other critical environmental parameters in space vehicles.

4.3 Flash Drive Integrated Label Free Silicon Nano-Photonic Bio-Assays for Space Station Bio-Diagnostics

Under the NASA STTR program, Omega Optics, Inc., University of Texas at Austin and George Washington University are developing label-free bio-assays in which TCC-VCSELs (Transverse-Coupled-Cavity- Vertical-Cavity Surface-Emitting Lasers) are integrated with photonic crystal (PC) microcavity lasers into a small and portable kit for space station bio-diagnostics and identification that can be measured by simple plug-and-play into an electrical measurement system. The effort offers an innovative and feasible approach to the NASA area of integrated photonic sensors (physical, chemical and/or biological), under the subtopic of PICs.

Table 1 compares our PC microarray platform with commercial Biacore SPR and fluorescence based ELISA systems.

Table 1: Comparison of broadly commercialized existing microarray platforms.

Company	Biacore SPR, Biacore 4000	ELISA	Omega Optics, Inc. PC Micro Array
Label-Free	Yes	No	Yes
Capture protein	3-10 µ-gram/ spot	100 µ-gram -1 mg/spot	<18 atto-grams/spot
Light Source	External	External	Chip-Integrated
Interaction Principle	Dynamic	Thermodynamic	Dynamic
Sensitivity	100 pM (1pM in Biacore 3000)*	0.01 pg/ml IL-17A (eBioScience)* 0.8 pg/ml IL-6 (Abcam)*	67 fg/ml demonstrated)
Sample Volume	60 micro-liters	50 micro-liters (eBioScience)*	0.3 nano-liters per spot

**All numbers are quoted from manufacturer data sheets available online.*

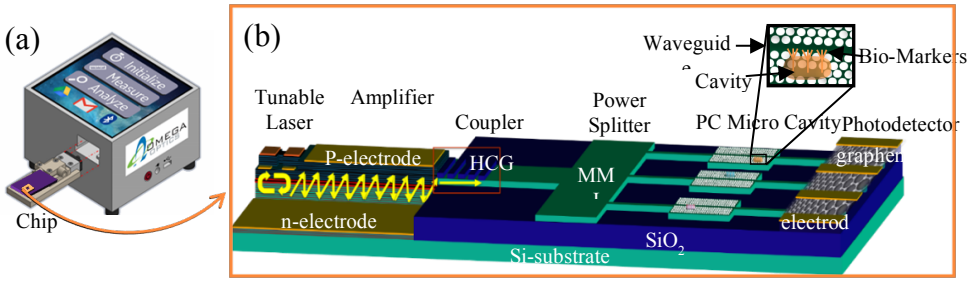

Figure 23. Flash drive integrated label-free Silicon nanophotonic bio-assay for space station bio-diagnostics. (a) Measurement system, and (b) Schematic of monolithically integrated tunable TCC-VCSEL for hand-held, low-weight, low-cost, label free silicon nano-photonic bio-assays for space station bio-diagnostics.

Advantageous of our proposed TCC-VCSEL microarray are 1) massively parallel, high throughput, miniature, label-free sensing of multiple biomolecules; 2) low analyte consumption, fast analysis and response times, simple optical measurement; 3) multiple biomolecule patterning exclusivity and target-probe biomolecule binding specificity; 4) an ideal platform for a personalized diagnostic device to analyze a variety of biomolecular (e.g. DNA, RNA etc.) chemical

and biological reactions on the same integrated platform with high throughput, thereby enabling rapid and specific diagnostics of bio-agents and infectious diseases.

4.4 Ultra-Compact On-Chip Integrated Spectrometers based on Metasurfaces

Spectrometers are powerful tools that are widely used in chemical and biological sensing, material characterization, and analysis of astronomical objects. The development of a high-resolution on-chip spectrometer could enable compact, versatile, energy-efficient spectroscopy for portable sensors as well as increasing lab-on-chip functionality. However, integrated spectrometers based on gratings require large footprints, while the ones based on holography have limited sensitivity. Here, we aim to address these critical challenges and to create an ultra-compact on-chip integrated spectrometer with high resolution, high sensitivity, and a small footprint via hybridization of integrated waveguides and newly emerging metasurfaces.

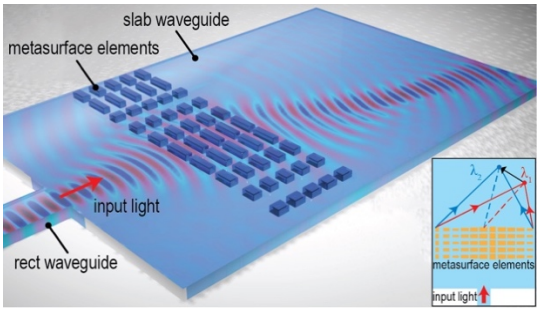

Figure 24. Metasurface integrated photonic spectrometer concept

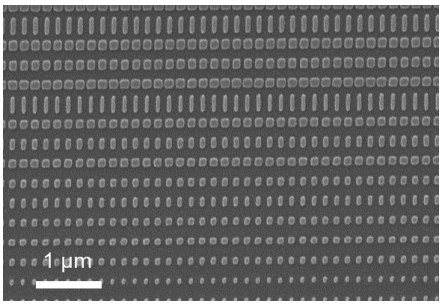

Figure 25. Scanning electron micrograph shows the metasurface region on a photonic integrated waveguide. The small particles are the meta-atoms (made of Si).

A metasurface is an ultrathin, engineered nanostructure that has the capability of locally tailoring the properties of light at the nanoscale. It offers tremendous power for manipulating light[24, 25, 26]. Nevertheless, metasurfaces usually designed to work for the light that propagates in the free space. Under an Early Career Faculty grant, the Pennsylvania State University, combined the metasurface with the photonic integrated waveguides by placing metasurface elements (i.e. meta-atoms) on the top of the waveguides (Figure 24). Through evanescent coupling, the resonating meta-atoms (Figure 25) will introduce abrupt phase shifts to the guided wave, so that we are able to control the guided optical modes. Exploiting a wavelength-sensitive configuration with those meta-atoms, the spectral information of the guided wave will be translated into an easily detectable quantity. Specifically, by distributing different meta-atoms on the waveguide, we are able to create a spatial phase profile for the guided light. With that, we can localize light with different wavelengths in different regions inside the waveguide. Therefore, the spectral information can be easily read out by photodetectors.

This research can lead to the technology transition of lightweight and portable systems for chemical and biological sensing, material characterization, and analysis of astronomical objects. In addition, it can be integrated into lab-on-chip applications to provide spectroscopic functionality. Besides, it can be used in photonic wearable devices for accurate health monitoring for astronauts. Furthermore, it can be naturally used as an integrated optical wavelength multiplexer / demultiplexer for board-to-board or rack-to-rack communications.

4.5 Monolithically Integrated TCC VCSELs with Surface-Normal 2D Slow-Light PC Waveguide Arrays

A light detection and ranging (LiDAR), is an optical remote sensing technology that quantifies effects of traveled light to cover a range of a distant target. Lidar can follow everything from airplanes to thunder-storms. LiDAR sensors require high-power laser for long distance detections (> 200 m). Under the NASA STTR program, Omega Optics, Inc., University of Texas at Austin and George Washington University are developing a new method based on Quality factor (Q) enhancing to achieve single-mode operation in transverse coupled cavity (TCC) vertical-cavity surface-emitting lasers (VCSELs). The main aspects of this method are as follows: (1) Single mode operation for the arrays with symmetric lasing profile, and (2) high power emission. In contrast to parity time (PT) single mode lasers where in which one of the cavities is lossy (and consequently does not lase), here all of cavities are lasing and none of them are lossy. In order to have an equitant array to have lower Q for all modes except for fundamental one, we engineer the main array in such a way that it has the lowest lasing threshold for fundamental mode. We adiabatically couple the array to the central cavity in such a way that it supports the fundamental mode of the main array and we increase the Q of this mode by adding extra gain to this central cavity. Next, the light propagates perpendicular to the bottom Indium Phosphide (InP)

substrate. In this part, a photonic crystal (PC) with a hexagonal lattice consisting of holes (air) arranged in a hexagonal lattice, surrounded by (InP), covered by a thin layer (10 nm) of ITO. The carrier density of the ITO film can be tuned in a capacitor configuration, ultimately altering its complex refractive index. The active modulation aims to produce a shift in the phase of the propagating wave, which travels parallel to the pillars and consequently molding its wave-front. This device concept can be used for novel space LIDAR technologies that use small and high-efficiency diode lasers to measure range and surface reflectance of asteroids and comets from >100 km altitude during mapping to <1 m. Figure 26 depicts our proposed concept. Instead of using 64 integration layers, we use vertically integrated PC waveguide arrays as shown in Figure 26(b), where each individual slow light PCW is shown in Figure 25(c). This will significantly increase the yield rate to the final targeted 98% since we have only one primarily defined lithography layer rather than a 64-layer approach without sacrificing the performance metrics.

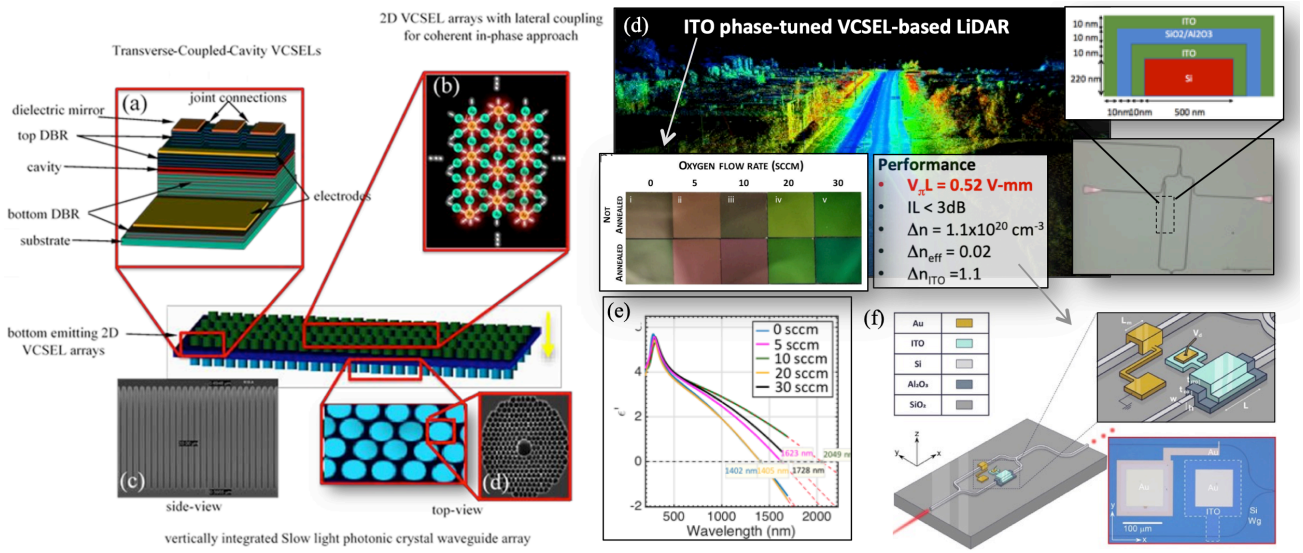

Figure 26. (a-d) Schematic of the TCC-VCSEL-based LiDAR core components featuring vertically integrated slow-light photonic crystal waveguide arrays that can provide the phase delay. (d) Beam steering is achieved by biasing a thin-film of ITO covering each individual laser cavity selectively to adjust the phase (see also Fig. 27). In brief, we tuned the ITO sputter process to produce a desired carrier-concentration for electro-static gating (carrier accumulation/depletion)[27]. With this we are able to achieve both process[24] and bias-based[28] ENZ films for voltage-efficient beam-steering across the c-band. (f) Demonstration of an efficient ITO-based phase shifter enabling $V\pi L$ = 0.52 V-mm[29].

Photonic crystal (PC) structures are periodically patterned materials with a strong dielectric contrast. In this case, 1 (air) to 3.15 @ 1550 nm wavelength (InP, Pettit et al). As illustrated in Figure 27a, in this case, the PC consists of patterned 4 µm deep holes in a substrate of InP. The holes are arranged in a honey comb fashion resulting in a hexagonal lattice with a hole radius d/2 =0.33Λ, being Λ=300 nm. Figure 27b represents the inverse lattice and points out the reciprocal vectors of the Bravais Lattice. Figure 27c sketches the computed lattice dispersion diagram showing normalized frequency versus the wave vector for transverse electric (TE) and transverse magnetic (TM) modes of the 2D photonic crystal. Here ω is the normalized frequency, which is expressed as ω=Λ/λ. It is worth mentioning that only TM modes are characterized by a band gap, which means that the PC forbids TM waves propagation within the highlighted frequency range. Engineering the specific band can be indeed determinant for controlling the light propagation inside a PC or coupling to subsequent devices, for filtering and improve Q factors. We change the carrier concentration of the ITO film in specific sections of the film in order to tailor the optical response of the system. The LiDAR system exploits separate and independent back-gating to achieve phase modulation by injecting carriers in the ITO film (Fig. 27d), highlighting two areas with different carrier concentrations N_1 and N_2. Three separate cases are addressed and presented; (i) only the portion of ITO on the right-hand side of the input port is modulated, reaching a concentration of 4×10^{20} cm^{-3} shows that the overall higher losses and lower refractive index of the right side forces the wave to be conveyed towards the left, with an angle of approximately 30 degrees, thus tailoring the wavefront of the transmitted radiation (Fig. 27e). (ii) Similarly, the carrier modulation intersects also the left part of the film, inducing a more pronounced deflection of the beam, up to 60 degrees (Fig. 27f). (iii) In symmetric modulation the thin film in correspondence of the impinging radiation (Fig. 27g); here an equal split of the optical power with a tilting angle of 30 degrees can be realized.

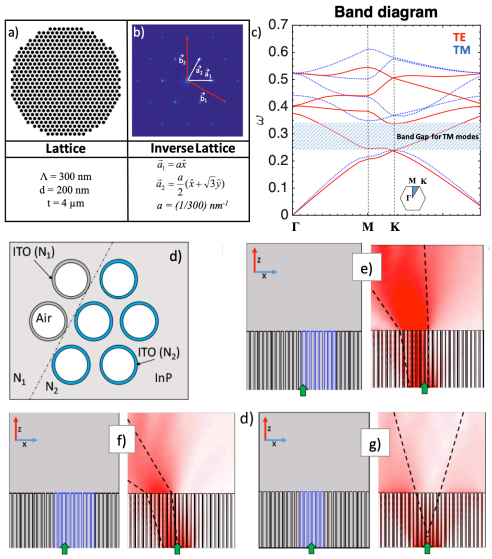

Figure 27. Characterization of the PC in the real (a) and reciprocal (b) space. c) Band diagram of the PC with hexagonal lattice. (d) Beam steering with selective modulation of the ITO film deposited on a PC. Schematic of the proposed mechanism. (e) Fully asymmetric, (f) Unbalanced and (g) symmetric modulation of the ITO carrier density with respect to the input port.

Subsequently, we analyzed the PC covered with a thin layer of ITO. For summarizing we will use a set of simulations in which we emphasized the possibility of engineer the physical parameters of a PC for obtaining desired band diagram and consequent spectral response. We observed that ITO modulation could be used for actively tuning the intensity of a propagating wave which crosses the PC based on our recent work on ITO optical-index tuning and carrier modulation . Moreover, we demonstrated that altering the carrier density in wisely chosen portion of the ITO film could lead to engineer the wave-front of the transmitted radiation but also represents a step forward in achieving compact power splitters and routers.

5. INTEGRATED PHOTONIC CIRCUITS FOR ANALOG RF APPLICATIONS

5.1 Tunable OEO based on photonic integration of ultra-high-Q resonators on a SiN chip

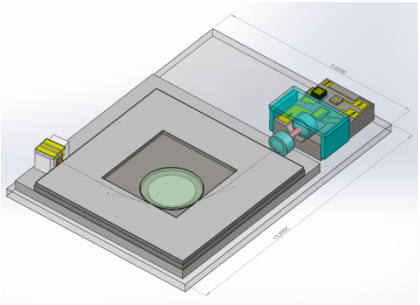

Figure 28. A design of the tunable microresonator-based OEO. A low insertion loss SiN waveguide suitable for coupling light in and out of the high-Q microresonator resonator has been designed and built.

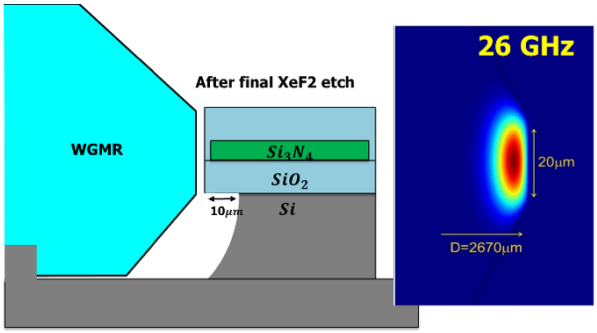

Figure 29. A design of a high-Q MgF_2 WGM resonator coupled with a low loss SiN waveguide. The waveguide is protruded on top of the silicon substrate to reduce leakage into substrate. Inset: field profile for the resonator.

A SiN-platform integrated photonic circuit suitable for a spectrally pure chip-scale tunable opto-electronic RF oscillator (OEO) that can operate as a flywheel in high precision optical clock modules, as well as radio astronomy, spectroscopy, and local oscillator in radar and communications systems is needed. The effort involved integration of an ultra-high quality (Q) crystalline whispering gallery mode (WGM) microresonator with multiple lithographically defined photonic and electronic components and devices (including a laser, a detector and waveguides) on a single platform with

nanometer-scale feature sizes. Ultimately the oscillator should be packaged in a volume of approximately 1cc, with net power consumption of less than 500 mW. The oscillator should produce a minimum of 10 mW of output RF power in Ka frequency band, and its single sideband phase noise should be as low as -60 dBc/Hz at 10 Hz, and -160 dBc at 1 MHz and higher Fourier frequencies.

RF oscillators and clocks are employed in virtually every electronic device, and are needed in a variety of NASA systems including radar, direction finding of signals of interest, and applications related to coherent operation across multiple segmented platforms. Phase noise, long term frequency stability, and SWaP parameters (size, weight, and power) are the basic characteristics of the oscillator. Advanced NASA applications require microwave and mm-wave frequency oscillators generating spectrally pure signals with stability at a level to function as the local oscillator in high performance atomic frequency standards. For these devices, the desired size is smaller than a quarter (25 Cent coin), with power consumption far less than a Watt.

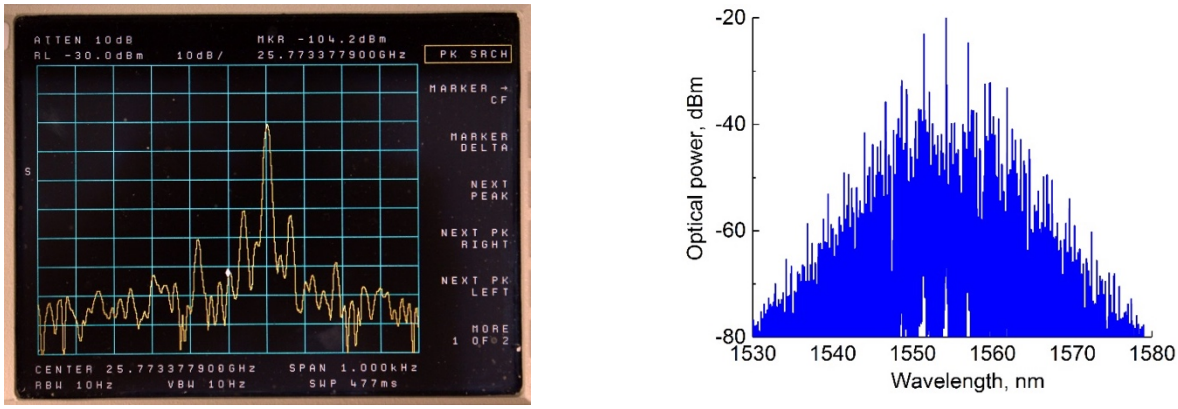

Figure 30: RF signal generated in the system. Spectrum of the RF signal (Left) created by the optical frequency comb (Right) on a fast photodiode.

Spectrally pure high frequency RF signals are usually produced electronically by multiplying the frequency of quartz oscillators or using dielectric resonator oscillators. Stability of simple free running electronic RF devices is limited both technically and fundamentally. The increasing complexity of stabilization circuitry as well as usage of external reference units, e.g. highly stabilized cavities, is typically required to improve phase noise of conventional electronic oscillators at small Fourier frequencies. It is desirable to develop a simpler stabilization technique for practical applications.

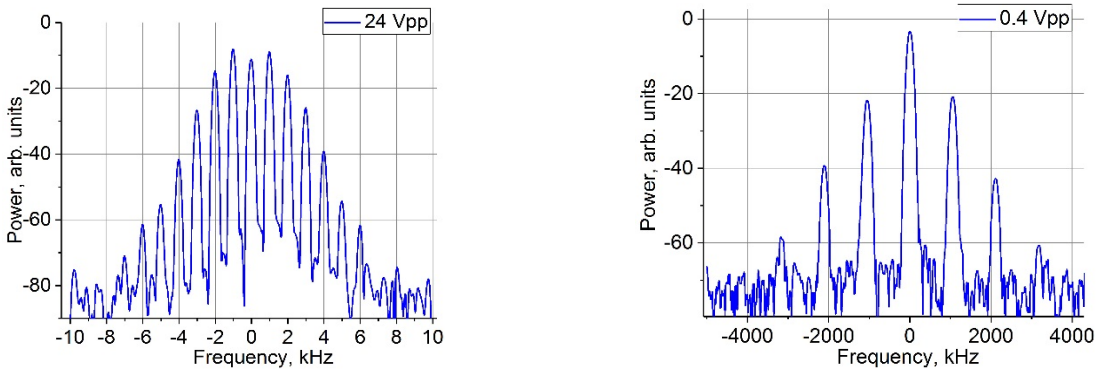

Figure 31: Spectra of the PZT modulated RF signals for 24 V (peak to peak), 1 kHz modulation frequency and 0.4 V (peak to peak), 1 MHz modulation frequency.

Photonic generation of RF signals provides an effective alternative solution to these challenges, adding new features to the oscillator, such as ultra-low phase noise[30], low power consumption, and small size. In this Phase I NASA STTR program, OEwaves Inc., along with a UC Davis team, designed an integrated tunable Ka-band oscillator based on hyper-parametric optical oscillations in crystalline whispering gallery mode (WGM) resonators[31,32]. These resonators are characterized with ultra-high Q[33], are compact and environmentally stable, and are ideal for realization of miniature,

high performance, RF photonic oscillators operating from X- to W- frequency bands and beyond. This approach will ultimately produce oscillators consisting of a semiconductor laser, resonator, and high-speed detector integrated in a chip-scale package.

We have demonstrated[34] a low noise optical frequency combs generation from a small OEO prototypes containing low loss (~1 dB) waveguide couplers of various shapes and sizes integrated with an ultrahigh-Q MgF_2 resonators. CMOS-compatible fabrication techniques yield low-loss optical waveguide couplers ideal for both in- and out-coupling of light to the high-Q resonators and for their subsequent integration with chip-on-submount semiconductor lasers (Figure 28). The waveguide design is illustrated by Figure 29. The team also demonstrated operation of the frequency comb generator based on the integrated resonator. The most important, modulation of the frequency comb repetition rate using a PZT actuator integrated with the resonator was validated.

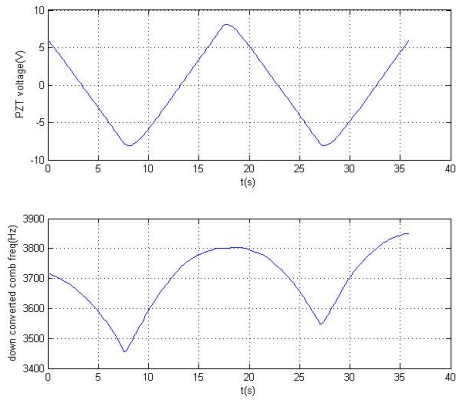

Figure 32: An example of nonlinear frequency modulation of the RF frequency. The nonlinearity is caused by the tuning of the operation point of the oscillator should be studied further.

We performed several experiments involving the frequency comb generation in the integrated resonator. The frequency comb was utilized for generation of the spectrally pure RF signals. The measurements are illustrated by Figure 30. The phase noise of the oscillator did not exceed -120 dBc/Hz at 10 kHz offset and -145 dBc/Hz at 10 MHz and higher offsets. PZT actuation of the RF signal frequency is illustrated by Figure 30. Interestingly, the frequency modulation sometimes was nonlinear, as shown in Figure 32. The reason is the complex mode interaction in the resonator. In some points the frequency comb repetition rate was independent of the stress applied by the PZT actuator. Similar points with temperature independent repetition rate frequency were observed. If tuned to this point the oscillator becomes independent on the environmental perturbations. This process will be further studied in the future.

ACKNOWLEDGMENTS

We gratefully acknowledge support from the NASA Early Career Faculty, Early Stage Innovation, Small Business Innovative Research and Small business Technology Transfer programs.

REFERENCES

[1] A. Chernikov *et al*., "Electrical Tuning of Exciton Binding Energies in Monolayer WS_2," *Phys. Rev. Lett.,* vol. 115, no. 12, p. 126802, (2015).

[2] D. Braga, I. Gutiérrez Lezama, H. Berger, and A. F. Morpurgo, "Quantitative Determination of the Band Gap of WS2 with Ambipolar Ionic Liquid-Gated Transistors," *Nano Lett.*, vol. 12, no. 10, p. 5218–5223, (2012).

[3] J. Fridlander, S. Pinna, V. Rosborough, S. Estrella, L. Johansson and J. Klamkin "RZ-DPSK photonic integrated transmitter for space optical communications," in Proc. *SPIE Photon. West*, 2018, Paper 10524-34.

[4] H. Zhao, S. Pinna, B. Song, L. Megalini, S. T. Šuran Brunelli, L. A. Coldren and J. Klamkin, "Indium Phosphide Photonic Integrated Circuits for Free Space Optical Links," in *IEEE Journal of Selected Topics in Quantum Electronics*, vol. 24, no. 6, pp. 1-6, Nov.-Dec. 2018.
[5] H. Zhao, S. Pinna, B. Song, S. T. Šuran Brunelli, B. Isaac, F. Sang, L. A. Coldren and J. Klamkin, "Widely tunable integrated laser transmitter for free space communications," in Proc. *International Semiconductor Laser Conference,* 2018, paper MC.5.
[6] H. Zhao, S. Pinna, B. Song, L. Megalini, S. T. Šuran Brunelli, L. A. Coldren and J. Klamkin, "3-Gbps Free Space Optical Link Based on Integrated Indium Phosphide Transmitter," in Proc. *IEEE Photonics Conference (IPC),* 2018, paper WA1.1.
[7] B. Song, C. Stagarescu, S. Ristic, A. Behfar, J. Klamkin, "3D integrated hybrid silicon laser," Optics Express 24(10), 10435-10444 (2016).
[8] K. S. Novoselov, V. I. Fal'ko, L. Colombo, P. R. Gellert, M. G. Schwab, and K. Kim. "A Roadmap for Graphene", Nature 490, 192-200 (2012).
[9] C. T. Phare, Y. H. D. Lee, J. Cardenas, and M. Lipson. "Graphene electro-optic modulator with 30 GHz bandwidth", Nature Photonics 9, 511-514 (2015).
[10] C. T. Phare, A. Dutt, A. Mohanty, and M. Lipson. "Integrated Graphene Electro-Optic Phase Modulator", CLEO 2017 Proceedings of the Conference on Lasers and Electro-optics STu3N.5 (2017).
[11] I. Datta, C. T. Phare, A. Dutt, A. Mohanty, and M. Lipson. "Integrated Graphene Electro-Optic Phase Modulator", CLEO 2017 Proceedings of the Conference on Lasers and Electro-optics STu3N.5 (2017).
[12] N. C. Abrams, M. Bahadori, C. T. Phare, M. Lipson, and K. Bergman. "Intermodulation Crosstalk of Graphene-Enable Electro-Optic Microring Modulators for DWDM Interconnects", OI 2017 Proceedings of the Optical Interconnects Conference (2017).
[13] X. Wang and S. Mookherjea, "Performance Comparisons between Semiconductor and Fiber Amplifier Gain Assistance in Recirculating-Frequency-Shifter" Optics Letters Vol. 43 No. 5, 1011-1014 (2018).
[14] X. Wang and S. Mookherjea, "Optimizing Recirculating-Frequency-Shifter performance with Semiconductor Optical Amplifier gain assistance" CLEO 2018 Proceedings of the Conference on Lasers and Electro-optics JW2A.63 (2018).
[15] P. O. Weigel, J. Zhao, D. Trotter, D. Hood, J. Mudrick, C. Dallo, A. Pomerene, A. Starbuck, C. DeRose, A. Lentine and S. Mookherjea, "Foundry-compatible Hybrid Silicon / Lithium Niobate Electro-Optic Modulator" CLEO 2018 Proceedings of the Conference on Lasers and Electro-optics SF2I.4 (2018).
[16] Y. Wang et. al., "Silicon/III-V Laser with Super-compact diffraction grating", Opt. Exp., Vol. 19, pp.2006 (2011)
[17] T. Li, D. Mao, N. W. Petrone, R. Grassi, H. Hu, Y. Ding, Z. Huang, M. Yu, G.-Q. Lo, D.-L. Kwong, J. C. Hone, T. Low, C. W. Wong and T. Gu, Spatially controlled electrostatic doping in graphene *p*-*i*-n junction for hybrid silicon photodiode, NPJ 2D Materials and Applications 2, 36 (2018)
[18] D. Mao, T. Kananen, J. Sinsky, N. W. Petrone, J. Hone, P. Dong, T. Gu, Bandwidth limitation of directly contacted graphene-silicon optoelectronics, ACS Applied Electronic Materials and Applications (2019)
[19] D Mao, T Kananen, J Sinsky, N Petrone, J Hone, P Dong, T Gu, Small-signal model for heterogeneous integrated graphene-silicon photonics, CLEO: Science and Innovations, SM2B. 4 (2018)
[20] O. J. Ohanian, A. A. Yakusheva, S. T. Kreger, D. Kominsky, B. J. Soller, M. Tran, T. Komljenovic, and J. E. Bowers, "OFDR on Photonic Circuits: Fiber Optic Sensing Infrastructure and Applications," in 26th International Conference on Optical Fiber Sensors, OSA Technical Digest (Optical Society of America, 2018), paper WB1.
[21] Fariah Mahzabeen, "Miniaturized Biosensor For Point-Of-Care Total Protein Measurement", Ph.D. dissertation, Dept. Elect. Eng., Stanford Univ., Stanford, CA, 2017
[22] J.S. Harris et al, Semicond. Sci. Technol., vol. 26, 2011
[23] Meredith M. Lee, "Tunable Photonic Crystal Biosensors For Portable Label-Free Diagnostics", Ph.D. dissertation, Dept. Elect. Eng., Stanford Univ., Stanford, CA, 2012
[24] N. F. Yu, and F. Capasso, "Flat optics with designer metasurfaces," Nature Materials 13(2), 139-150 (2014).
[25] A. V. Kildishev, A. Boltasseva, and V. M. Shalaev, "Planar Photonics with Metasurfaces," Science 339(6125), (2013).
[26] S. Chang, X. Guo, and X. Ni, "Optical Metasurfaces: Progress and Applications," Annual Review of Materials Research 48(1), 279-302 (2018).
[27] Y. Gui, M. Miscuglio, Z. Ma, M. T. Tahersima, V. J. Sorger „Impact of the process parameters to the optical and electrical properties of RF sputtered Indium Thin Oxide films: a holistic approach," ***arXiv:*** 1811.08344 (2018).

[28] V. J. Sorger, D. Kimura, R.-M. Ma and X. Zhang „Ultra-compact Silicon nanophotonic Modulator with broadband Response," Nanophotonics 1, 1, 17-22 (2012).
[29] R. Amin, R. Maiti, C. Carfano, Z. Ma, M.H. Tahersima, Y. Lilach, D. Ratnayake, H. Dalir, V.J. Sorger, "0.52 V-mm ITO-based Mach-Zehnder Modulator in Silicon Photonics," APL Photonics**,** 3,12 (2018).
[30] T. M. Fortier, M. S. Kirchner, F. Quinlan, J. Taylor, J. C. Bergquist, T. Rosenband, N. Lemke, A. Ludlow, Y. Jiang, C. W. Oates & S. A. Diddams, "Generation of ultrastable microwaves via optical frequency division," Nature Photonics 5, 425 (2011).
[31] T. J. Kippenberg, S. M. Spillane, and K. J. Vahala, "Kerr-Nonlinearity Optical Parametric Oscillation in an Ultrahigh-Q Toroid Microcavity," Phys. Rev. Lett. 93, 083904 (2004).
[32] A. A. Savchenkov, A. B. Matsko, D. Strekalov, M. Mohageg, V. S. Ilchenko, and L. Maleki, "Low threshold optical oscillations in a whispering gallery mode CaF2 resonator," Phys. Rev. Lett. 93, 243905 (2004).
[33] A. A. Savchenkov, A. B. Matsko, V. S. Ilchenko, and L. Maleki, "Optical resonators with ten million finesse," Opt. Express 15, 6768 (2007).
[34] G. Liu, V. S. Ilchenko, T. Su, Y.-C. Ling, S. Feng, K. Shang, Y. Zhang, W. Liang, A. A. Savchenkov, A. B. Matsko, L. Maleki, and S. J. B. Yoo, "Low-loss prism-waveguide optical coupling for ultrahigh-Q low-index monolithic resonators," Optica 5, 219-226 (2018).